Construction and Building Materials 124 (2016) 826–837

Contents lists available at ScienceDirect

Construction and Building Materials

journal homepage: www.elsevier.com/locate/conbuildmat

The use of geogrid reinforcement for enhancing the performance of concrete overlays: An experimental and numerical assessment

Hayssam Itani, George Saad *, Ghassan Chehab

Department of Civil & Environmental Engineering, American University of Beirut, Lebanon

HIGHLIGHTS

- Experimental setup to assess performance of geogrid reinforced PCC overlays.
- Geogrid reinforcement leads to crack resilient overlays with substantial ductility.
- Geogrids control the crack growth rate and prevent complete failure of PCC overlays.

ARTICLE INFO

Article history:
Received 13 April 2016
Received in revised form 2 August 2016
Accepted 4 August 2016
Available online 8 August 2016

Keywords:
Concrete overlays
Reflective cracking
Pavements
Geogrids
FEM

ABSTRACT

The use of thin concrete overlays as a rehabilitation option of existing distressed pavements is, similar to other overlay options, prone to the phenomenon of reflective cracking. Being a thin layer, consisting of thin Portland cement concrete (PCC), and lacking reinforcement allows the cracks in existing pavements to propagate through the concrete due to the horizontal and vertical movement of the underlying layer. This study investigates the use of geogrids as a reinforcement-crack arresting layer in thin concrete overlays to enhance their performance by: (1) providing additional tensile strength, (2) ductility, and more importantly: (3) controlling crack propagation to mitigate reflective cracking. Two experimental setups are utilized to assess and quantify the effect of inclusion of the geogrids for mode I cracking: the direct tension test to simulate thermal loads, and the flexure test to simulate the traffic loads. The outcomes from these experiments are then used to calibrate finite element models simulating the behavior of geogrid reinforced overlays under the above conditions. The FEM models are used to study the sensitivity of varying the location of the geogrid reinforcement. The obtained results verify that the use of geogrid reinforcement significantly enhances the overlay performance in the post-cracking regime in terms of strength, ductility and mode of failure.

1. Introduction

Placing a structural concrete overlay atop existing pavements is a conventional rehabilitation method of distressed PCC pavements. This type of maintenance is considered cost-effective and can be used for almost any combination of existing pavement type and condition, desired service life and anticipated traffic loading. Concrete overlays are widely used because they offer many benefits, including increased load carrying capacity, extended service life, fast construction and low maintenance requirements [1]. However, reflective cracking in the new overlay has been a serious challenge associated with pavement rehabilitation, and it is one of the most common failure modes of roads [2]. Reflective cracking involves the development of cracks in the new overlay that mirror the cracks and/or joints in the old existing pavement [3]. Al-Qadi et al. [4] presented three different cracking modes of pavement sections: Mode I cracking (Opening mode) resulting from thermal and traffic loading that are applied normally to the crack plane; Mode II cracking (Sliding mode) resulting from traffic loading causing in-plane shear loading; and Mode III cracking (Tearing mode) resulting from out-of-plane shear loading.

The external wheel load leads to high stress and strain in the overlay above the existing crack where the bending stiffness of the rehabilitated pavement section is reduced due to the discontinuity in the existing pavement creating stress concentration [5]. When the stress value exceeds the fracture resistance of the overlay, a crack is initiated and a combination of mode I and II leads to crack propagation through the overlay [6]. Moreover, the

* Corresponding author.
E-mail addresses: hmi11@mail.aub.edu (H. Itani), george.saad@aub.edu.lb (G. Saad), ghassan.chehab@aub.edu.lb (G. Chehab).

http://dx.doi.org/10.1016/j.conbuildmat.2016.08.013
0950-0618/

movement of the discontinuous underlying pavement caused by temperature changes results in additional concentrated tensile stresses in the new pavement above the existing crack or joint; this phenomenon is directly related to the mode I crack opening mechanism [7].

Due to the number of variables that are involved in the mechanism of reflective cracking, various solutions for mitigating or delaying reflective cracking have been suggested by researchers, yet complete prevention of their occurrence has proven difficult. For instance, it has been shown that incorporating geosynthetic materials as part of the overlay system in rehabilitation of pavements enhances the performance and extends the service life of pavements prone to reflective cracking [5]. In fact, geosynthetics have long been used to enhance the performance of engineering structures, in particular for geotechnical applications [8], as they are used as reinforcing and stabilizing agents in various heavy civil and infrastructure works [9,10]. Geogrids are a particular type of geosynthetics formed in a stiff grid like structure with large apertures [10]. Geogrids have been widely used as reinforcement in structures with unbound materials, such as pavements, slopes, retaining walls, and embankments. Given a proper ratio of geogrid aperture size to aggregate grain size, geogrids provide lateral confinement to the pavement aggregate base course through shear resistance and friction between the geogrid and surrounding aggregate [11]. Most geogrids are made from woven textile or from extruded polypropylene, and could vary in physical and mechanical properties, particularly stiffness and strength. While uniaxial geogrids are mostly used for slope stability, biaxial geogrids are used in applications where biaxial stresses prevail such as in pavements [12].

In pavements applications, geosynthetics are usually employed as anti-reflective cracking systems in asphalt pavements [13,14]. They restrain the lateral movement of the aggregate layers under traffic loading by confining those layers [15]. They have also been used as reinforcements in asphalt pavement layers resulting in reduction of fatigue cracking [16]. Guo and Zhang [17] investigated the geogrid-reinforced asphalt overlays and found it to be effective in controlling cracks when placed at the bottom of the overlay and increasing the overlay's fatigue life by 80%. Little investigation however has been done on the use of geogrid as main reinforcement in thin Portland cement concrete elements, such as overlays in pavements, where the use of steel reinforcement is not possible [18]. El Meski and Chehab [19] have conducted an experimental study on the flexural behavior of geogrid reinforced concrete beams and they concluded that the use of geogrid as reinforcement in concrete provide a ductile post-cracking behavior, high flexural strength and fracture energy, and large deflection.

The objective of this study is to evaluate and quantify the effectiveness of using geogrids in thin concrete overlays to mitigate reflective cracking caused by applied wheel loads and temperature fluctuations. To achieve this objective, two experimental setups are designed to assess and quantify the effect of inclusion of the geogrids in Portland cement concrete overlays under mode I cracking. The direct tension test is conducted to simulate thermal loads while the flexure test is used to simulate the traffic loads. The outcomes from these experiments are then used to calibrate finite element models simulating the behavior of geogrid reinforced overlays. The FEM models are used for sensitivity analyses to study the effects of varying the location of the geogrid reinforcement on the strength of the overlays. The outcomes of this assessment provide a better understanding of the mechanisms behind the reinforcing performance and important factors influencing it. Evaluated behavioral aspects of geogrid-reinforced concrete overlays include maximum load capacity, load-deflection response, flexural displacement, crack propagation rate, flexural strength, and mode of failure.

2. Experimental setup

In design and construction of PCC overlays, it is essential to study the behavior of the utilized concrete in tension due to the significant failures associated with reflective cracking phenomena, that is in turn heavily associated with the tensile behavior of the overlay [20]. Two experimental setups are designed to assess and quantify the effect of inclusion of the geogrids in Portland cement concrete overlays: the direct tension test to simulate thermal loads and the flexure test to simulate the traffic loads. Both tests were conducted on PCC specimens at room temperature using a hydraulic, closed loop Universal Testing Machine, UTM-25 by IPC, having a capacity of 25 kN and a 16-bit control and data acquisition system.

2.1. The direct tension test

The direct tension test of concrete, although of considerable interest, has been given little attention by researchers due to the difficulties in applying direct tension loading to concrete specimens. Alternatively, the indirect tension test (Brazilian test) and beam flexure test (3 point or 4 point bending) were mostly used to study the tensile properties of concrete. The tensile properties of concrete are important in the study of mitigating reflective cracking, since concrete layers are subjected to tensile stresses, such as those associated with temperature differentials and drying shrinkage [20]. The direct tension test is usually conducted by fixing one end of a specimen and applying a displacement to the other end through an actuator. Typically, the ends are fixed by either using clamps [21], gluing with epoxy, or by casting steel studs into the concrete specimen [22]. However, these methods suffer from a major problem related to inducing secondary stresses at the ends causing uneven stress distribution and localized failure [23].

To alleviate the stress concentration due to the end effects, the cross-sectional area of the specimen at the ends should be larger than that in the middle of the specimen where cracking is desired to happen, and where Linear Variable Differential Transducers (LVDTs) are placed for uniform strain measurement [19]. For that purpose, an FEM model of the direct tension test was developed using the Automatic Dynamic Incremental Nonlinear Analysis "ADINA" [24] software to come up with the optimal specimen configuration. The FEM mesh used consists of three dimensional solid elements with eight (8) nodes each. The constitutive material model for concrete used is a nonlinear, multi-axial constitutive model which has the characteristic of failing in tension at a maximum, relatively small, tensile stress and a crushing failure due to high compression [24]. The following parameters are defined for the concrete material: Tangent modulus at zero strain, Poisson's ratio, cut-off and post cracking tensile stress, maximum compressive stress and strain and ultimate compressive stress and strain. The mesh size was selected to be 5 mm. It is important to note that the goal of the FEM model is to examine stress concentration effects only and not to study failure limits. To that extent the material properties and loading regimes are not of significant importance. Nevertheless, a prescribed displacement was used for loading the model, at a rate of 0.0133 mm/s, and an incremental solution process was adopted using the full Newton iteration method. Based on the FEM study, it was decided to use a notched dog bone shaped sample with 14 mm steel threaded rods embedded within the concrete as shown in Fig. 1a. The FEM trials results show that the adopted configuration has the ability to distribute the tensile stresses almost uniformly at the notched section location as shown in Fig. 2a, where the tensile stresses are within ±1.75% of the average stress. The height of the samples is 40 cm

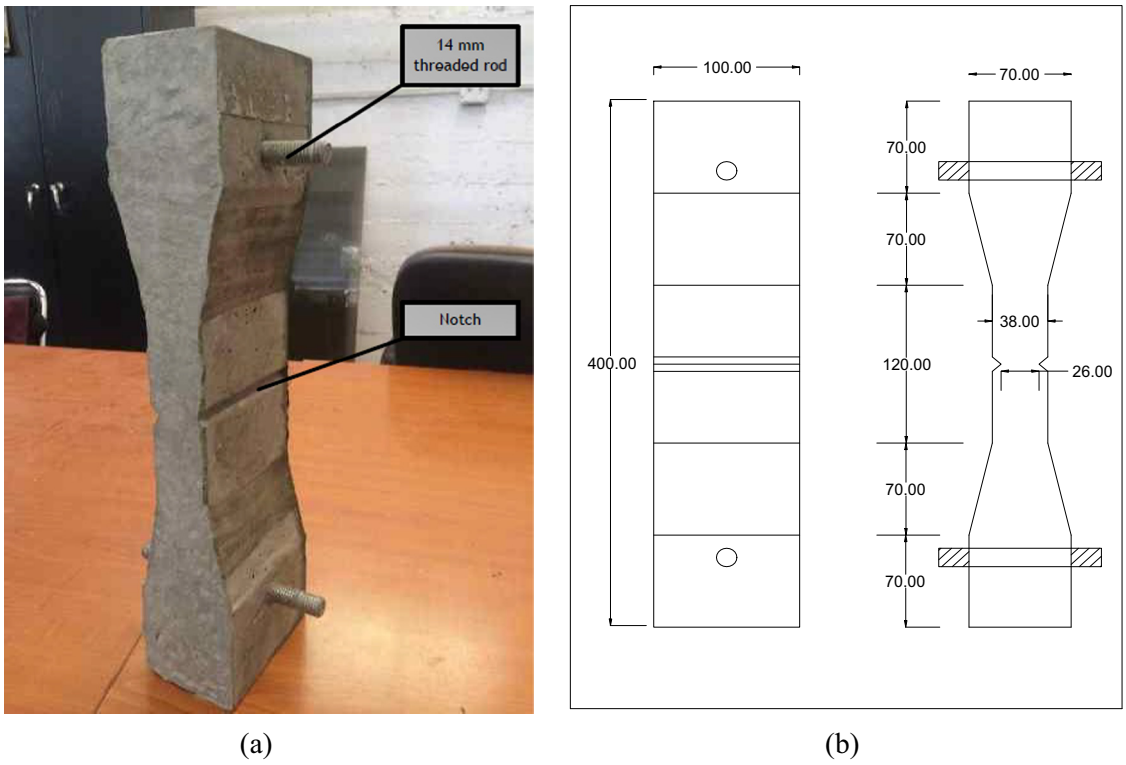

Fig. 1. (a) The notched dog bone specimen used for the direct tension test. (b) Exact dimensions used for specimen preparation.

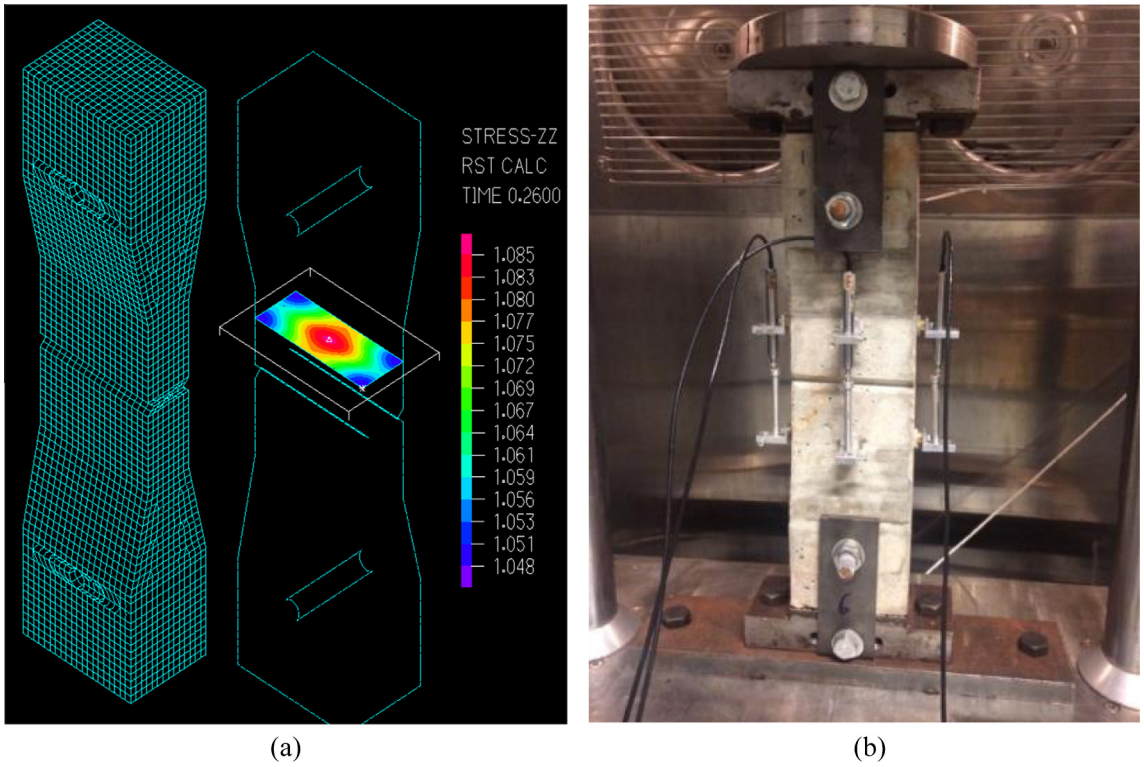

Fig. 2. (a) FEM model results showing the tensile stress distribution (MPa) at the reduced section where the strain is measured. (b) The direct tension test setup.

with the largest cross sectional area (7×10 cm) at the top and bottom, a reduced section (3.8×10 cm) in the middle below and above the notch, and the smallest section at the notch (2.6×10 cm) as shown in Fig. 1b. The threaded rods are to be used for applying the load and fixity on the specimens. An assembly of steel plates is designed to fix the specimen with the machine from the actuator and the base sides. Fig. 2b shows the adopted concrete specimen and the final testing setup.

Wooden molds were fabricated for the specimens. To create the reduced area in the middle, another beveled piece of wood is attached to the sides. To create a triangular notch, a strip of Plexiglas was glued on the sides of the mold at mid height; the cross section of the notch is 11.2 mm wide and 5.8 mm deep. The sides of the molds were drilled to install the 14 mm threaded rods. The layer of geogrid is then installed in the longitudinal section along the height of the specimen. For casting the geogrid reinforced samples, layers of concrete were poured and compacted with a steel rod.

Six specimens were prepared for testing. Among the prepared specimens, three were made of plain concrete with no reinforcement to serve as control, while the others were reinforced with uniaxial geogrid of high tensile strength placed along the middle longitudinal section. For all tested specimens, the load is gradually applied in displacement control mode at a constant rate of 0.0133 mm/s until failure.

2.2. The flexure test

The flexure test was specifically designed to evaluate the effects of using geogrids to reinforce overlays under bending mode (mode I). The proposed setup consists of a PCC slab (380 mm length, 150 mm width, and 50 mm thickness) notched along its width at the middle section of the slab from edge to edge to induce stress concentration for crack initiation and subsequent propagation. For reinforced slabs the geogrid was placed at 1/3rd the thickness from the bottom. A 30 mm thick neoprene rubber base with an elastic modulus of 100 MPa was placed under the slab to simulate the effect of deteriorated pavement layer or an aggregate base layer. The loading was applied on the top center of the concrete slab through a circular loading plate (138 mm diameter). A soft rubber pad is placed between the steel plate of the actuator and the concrete to allow for uniform distribution of the load on the specimen and simulate the rubbery surface of a wheel load.

Fig. 3 shows the testing setup for the flexure test. Wooden molds were fabricated for the slab specimens. To create a triangular notch, a strip of Plexiglas was glued to the bottom of the mold at mid length; the cross section of the notch is 11.2 mm wide and 5.8 mm deep. For casting the geogrid reinforced samples, one third the depth of the concrete layer was first poured and compacted with a steel rod. Then, the geogrid layer was carefully installed in the mold. Another layer of concrete was later poured above the geogrid, ensuring that proper mixing between the two concrete layers above and below the geogrid occurs. No separation between the layers and no surface voids were observed after de-molding the samples.

Two types of loading were adopted for this test setup: monotonic and cyclic loading. For the monotonic case, the load was applied at a constant rate of 0.216 kN/s until failure. To simulate moving traffic wheel loading, a cyclic load was applied to the specimens using a hydraulic dynamic loading frame. To model a truck wheel load the cyclic load was set to result in a pressure of 690 kN/m^2 (100 psi). A 50 kN/m^2 minimum pressure was used to keep the loading plate in place during dynamic loading. The loading wave shape was haversine, and the loading was applied with a frequency of 10 Hz to simulate high speed traffic.

A total of 12 notched slab specimens were cast for the test; six of them were tested under monotonic loading and the remaining under cyclic loading. Among each of the six specimens, three of them were plain concrete to serve as control samples and the other three were reinforced with uniaxial geogrid.

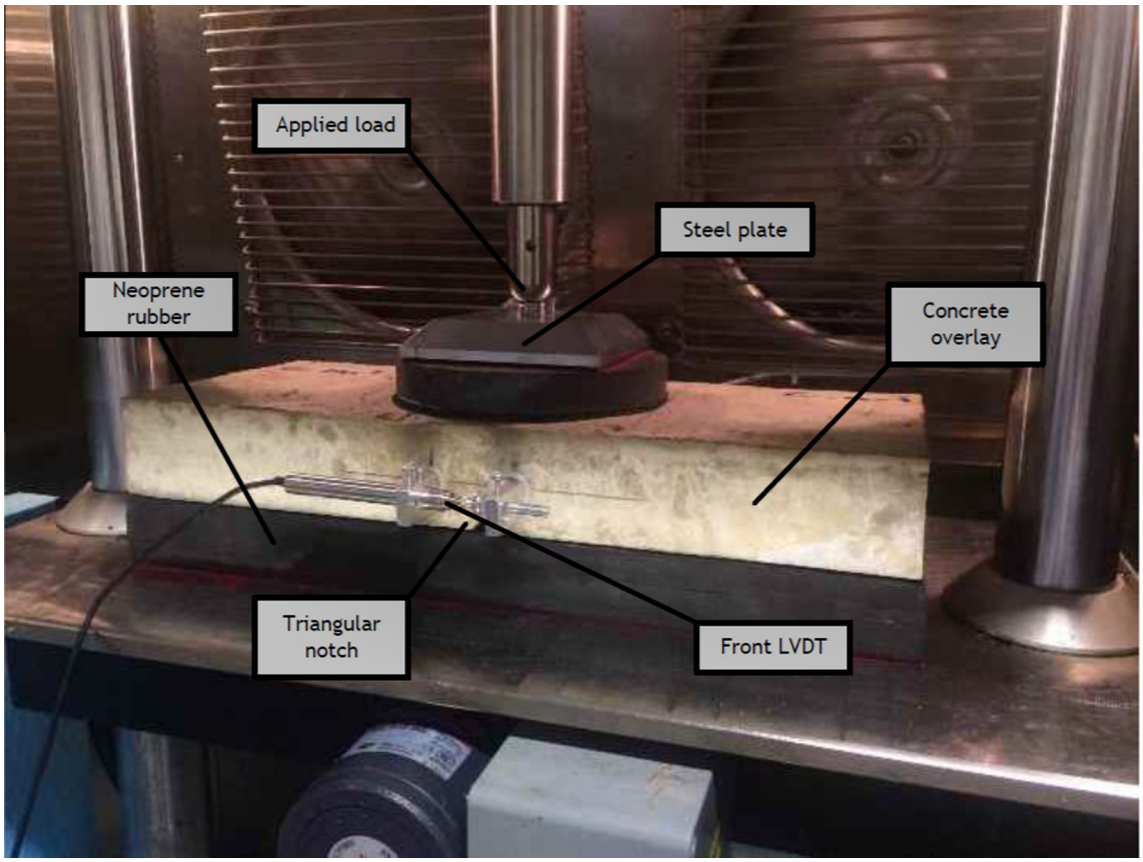

Fig. 3. The flexure test setup.

2.3. Measurement instrumentation

Linear Variable Differential Transducers (LVDTs) were used to measure the displacements. For the direct tension test, they were fixed to steel targets glued to the sides of the specimen to measure the axial deformation. As for the flexure test, the LVDTs were measuring the flexural opening displacement at the notch (Δf). They were installed on both sides of the specimen at a distance of 20 mm from the bottom of the sample. The readings from the LVDTs were averaged for use in the analysis.

2.4. Material properties

Type I Portland cement, natural sand and medium size limestone with a nominal maximum aggregate size of 9.5 mm were used for the concrete mix. The used sand was dry and the aggregates were cleaned from the dust and fine particles. The concrete mix was designed to produce a cylindrical concrete compressive strength of 27 MPa at 28 days. The specimens were placed in a curing room for 15 days with continuous wetting cycles at a temperature of 23 ± 5 °C and relative humidity greater than 95%. The maximum aggregate size of the PCC mixture was smaller than the aperture dimensions of the uniaxial geogrid. Such condition provides adequate interlock and prevents potential blocking by allowing all aggregates to pass through the aperture of the geogrid.

A typical uniaxial geogrid specimen is shown in Fig. 4. The physical and mechanical properties of the used geogrids were obtained from the manufacturer and are presented in Table 1. Moreover, to better understand the behavior of the geogrids, a uniaxial tension test was conducted on four replicates of the uniaxial geogrids to characterize their mechanical properties.

Fig. 5a shows the setup used for testing the uniaxial geogrids. Friction grips were used to hold the geogrid at the junction location, and load was applied gradually until failure. Fig. 5b shows the engineering stress, obtained by dividing the applied load by the initial specimen cross-sectional area, against the engineering strain, obtained by dividing the specimen deformation by the original length. As seen, there is excellent repeatability in testing and uniformity in mechanical behavior across samples. The average value for the geogrid modulus of elasticity at low strains (linear range) was found to be 2290 MPa. A comparative analysis shows similarity between experimental results and the manufacturer properties in terms of modulus of elasticity and peak tensile strength.

Fig. 4. A typical uniaxial geogrid specimen.

Table 1
Physical and mechanical properties of the used uniaxial geogrids.

Component	Description	Unit
Polymer type	HDPE	–
Aperture size MD	220	mm
Aperture size TD	13/20	mm
Mass per unit area	1000	g/m2
Strength at 2% strain	45	kN/m
Strength at 5% strain	90	kN/m
Peak tensile strength	160	kN/m
Yield point elongation	13	%
Junction strength	130	kN/m
Long term design strength	75.4	kN/m

Note: MD = machine direction; TD = transverse direction.

3. Results and analysis

3.1. The Direct tension test

During the test, loading was applied gradually at a constant rate of 0.0133 mm/s. Once the stress in the concrete reached its strength value, a crack initiates at the location of higher stress which is the notch. Fig. 6a shows a typical plain concrete failed specimen, the ending of the test was signified by the complete failure of the concrete specimen; splitting it in half. This behavior is attributed to the brittle failure of plain concrete. Whereas for reinforced samples, in the elastic range, the concrete and the geogrids are working together to resist tensile stresses; after cracking, complete failure of the concrete takes place at the fractured surface. At this stage, only geogrids will resist the applied displacement load since concrete loses its tensile load bearing ability post failure. This is clearly shown in Fig. 6b which depicts a typical geogrid reinforced concrete failure mode. It is worthy to mention that during testing and analysis it was noticed that the LVDT's on both sides of the specimen were recording similar readings. This is a good indication that the specimen is not tilting and the load is distributed uniformly over the area.

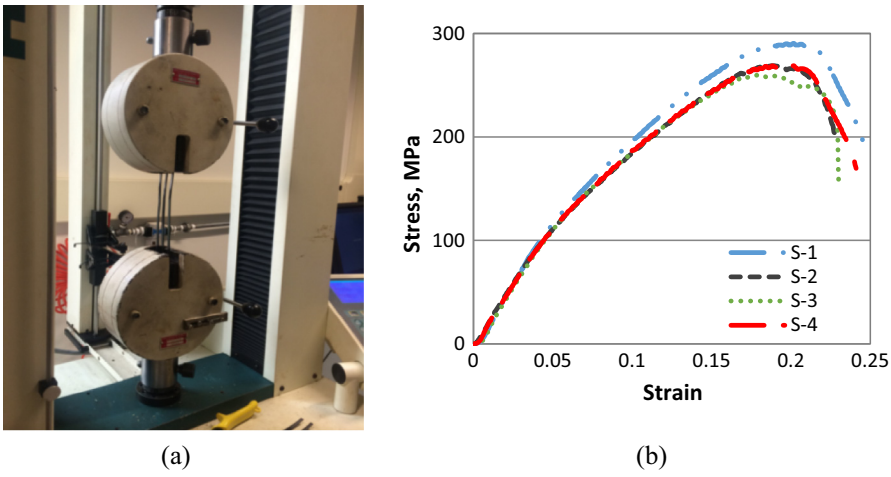

Fig. 5. (a) Testing setup for the geogrid samples. (b) Engineering stress (MPa) vs. strain curves for the four test samples of geogrids.

Fig. 6. (a) Typical plain concrete failure mode; (b) typical geogrid reinforced concrete failure mode.

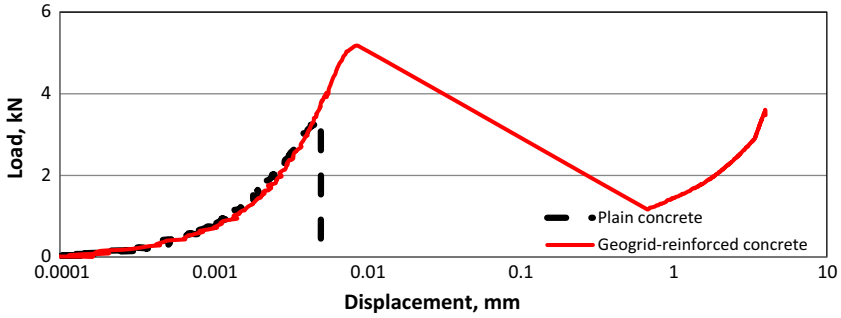

Fig. 7. Average load vs displacement of the plain and geogrid reinforced samples (based on 3 replicates each).

Fig. 7 presents the average load-deflection curves for both plain and geogrid-reinforced concrete samples (3 each) tested according to the direct tension test setup described earlier. Just after initial cracking of concrete, both exhibit sudden drop in load. As for the failure mode, the plain concrete specimens follow a brittle failure due to the lack of any reinforcement. However, the geogrid-reinforced samples exhibit cracking delay and an increase in strength after cracking. It is also shown from Fig. 7 that the geogrid-reinforced samples undergo significant deformation after initial cracking due to the geogrid ductility. This extensive deformation shows that the inclusion of geogrid provides post cracking ductility.

It is noticeable from Figs. 7 and 8 that the maximum load capacity of the geogrid-reinforced sample is greater than that of plain concrete. The fracture behavior of concrete is determined by the interaction between the strength and stiffness of the different components of concrete (i.e. cement matrix, aggregate) [21]. Usually cracks start at the weakest zone in concrete which is the matrix-aggregate interface and then propagate. After that, the crack may encounter a coarse aggregate that can be either fractured or can generate toughening mechanisms [21]. The crack will always propagate in the direction that requires the least work. The geogrid layer, which is placed in the middle of the specimen, is affecting the path of the crack; therefore, the required energy is higher in the case of geogrid reinforced concrete than the plain concrete, thus the higher load capacity. The fracture energy is defined by the area under the load-displacement curve. The more required energy for a crack to open the more resilient the section

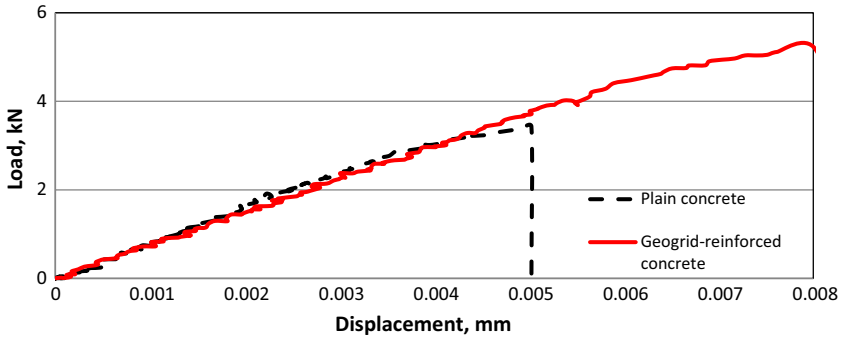

Fig. 8. Average load vs displacement of the plain and geogrid reinforced samples at low displacement levels (based on 3 replicates each).

is. As shown in Fig. 8 the inclusion of the geogrid leads to an increase in the fracture energy.

3.2. The flexure test

For monotonic and cyclic loading, the test was conducted until the vertical crack propagated the full depth of the overlay and reached the top of the specimen. When this was not applicable, the test was terminated due to the machine capacity restriction.

Fig. 9 shows the evolution of crack starting by initiation from the tip of the notch, widening and further propagation. The screen shots were taken from a recorded video which was played in slow motion. It is worthy to mention that the starting point of the crack in all the specimens was the notch, and no cracks were observed away from the notch.

3.2.1. Monotonic loading test results

After loading, two phases are identified: the pre-cracking and post-cracking phase separated by an initial cracking point. After the initial cracking, a sudden and significant increase in Δf was witnessed. Then the crack started widening and propagating upwards. It is noticed from Fig. 10, which is obtained by averaging the results of three test replicates, that the rate of crack opening in the plain concrete is higher than the geogrid reinforced one in the post-cracking phase. For example, at a load of 20 kN the Δf of plain and reinforced concrete are 0.7 and 0.43 mm respectively, which means 38.5% decrease in the Δf. The load is redistributed to the geogrids after initial cracking of concrete; therefore, the resistance against crack opening in the geogrid sample will be higher than plain concrete resulting in smaller values of Δf.

However, in the pre-cracking phase, as shown in Fig. 11, the notch flexural opening displacement in the geogrid reinforced samples are higher than the plain concrete and the initial cracking always occurs before in the geogrid reinforced samples (6.0 kN for geogrid and 8.4 kN for plain concrete). This is attributed to the fact that the presence of geogrids is weakening the section of the overlay by dividing it into an upper part and lower part instead of allowing it to act as a whole while resisting bending stresses.

The machine maximum load limit is 23 kN, at which point the loading is stopped. For unreinforced specimens, as loading is applied, the crack initiates at the notch location and propagates upwards to the surface of the specimen causing total split of the specimen into two halves. Whereas, for geogrid-reinforced specimens, cracks did initiate earlier on during loading; however, after preliminary propagation the geogrid acts as a crack arrestor and stops the crack at the location of the geogrid layer below the neutral axis of the specimen. As such, the crack does not propagate all the way to the surface of the specimen, thus the specimen remains

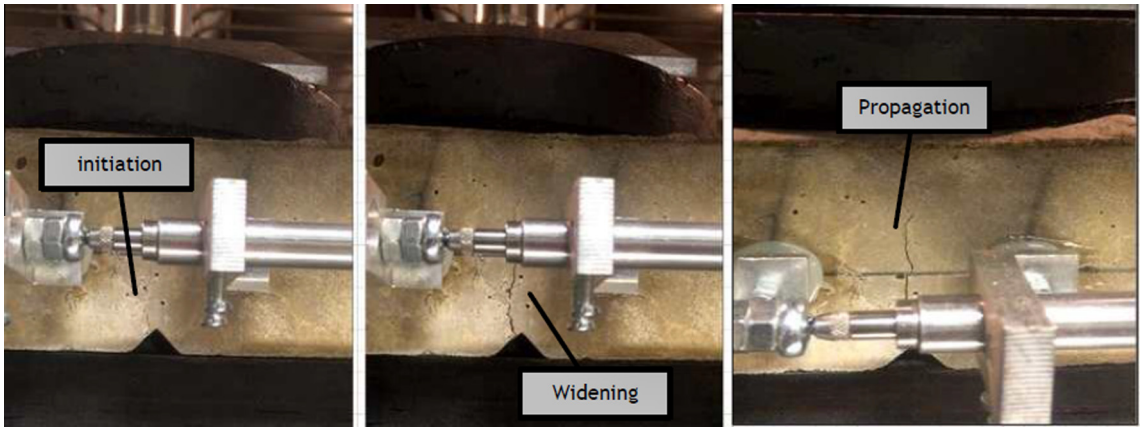

Fig. 9. Crack initiation, widening and propagation from the tip of the notch.

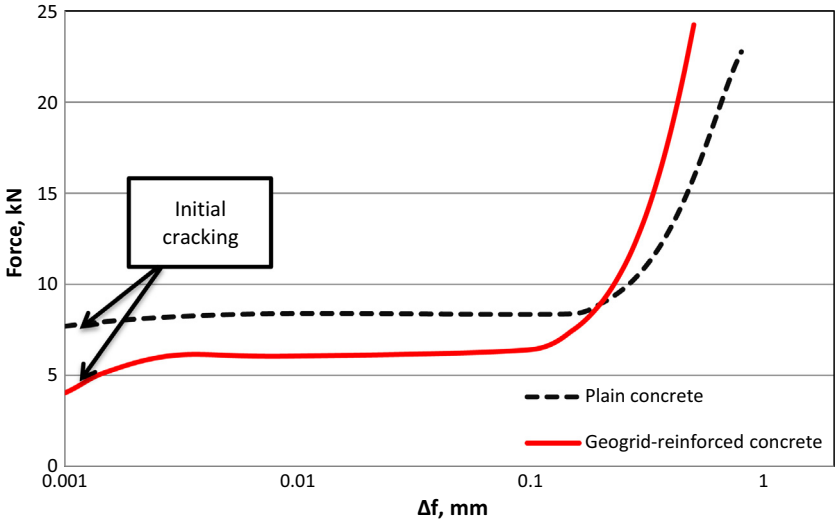

Fig. 10. Average load vs. Δf for the plain and geogrid-reinforced concrete samples for the post cracking phase (based on 3 replicates each).

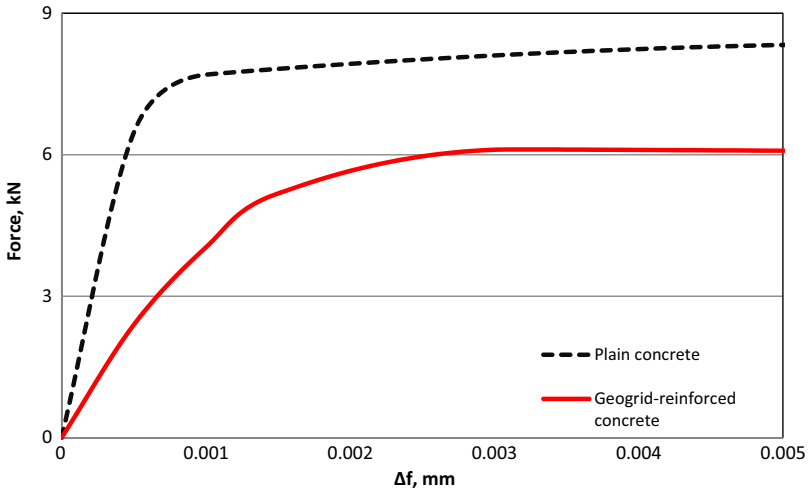

Fig. 11. Average load vs. Δf for the plain and geogrid-reinforced concrete samples for the pre-cracking phase (based on 3 replicates each).

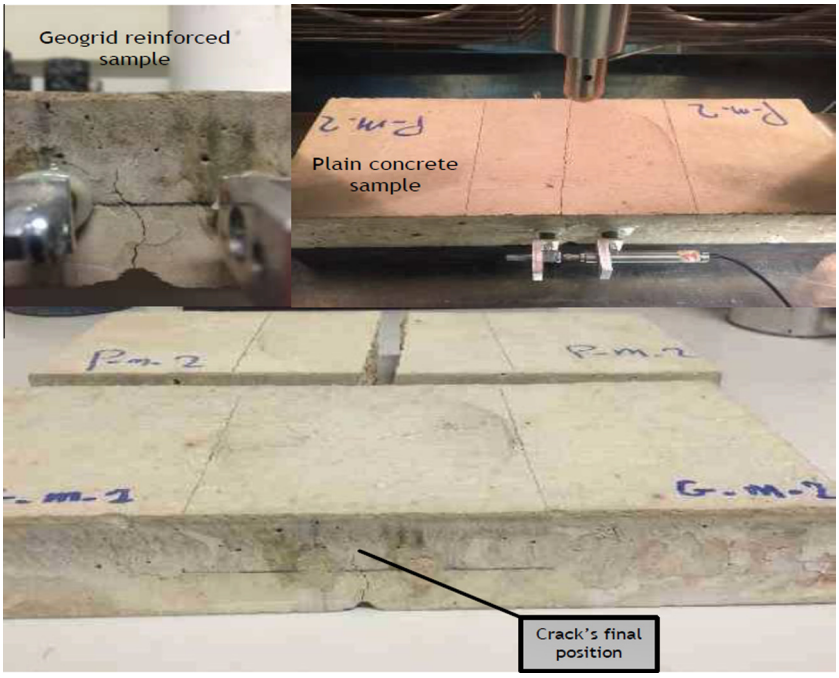

Fig. 12. Crack propagation and failure in plain vs. geogrid reinforced concrete.

intact in one piece. Fig. 12 shows typical failure modes of plain concrete and geogrid reinforced concrete samples.

3.2.2. Cyclic loading test results

In this testing protocol, the same test setup described above was used, and a total of 100,000 load cycles were applied at a frequency of 10 Hz without rest period. The test was either stopped when the 100,000 cycles finished or when complete failure of the specimen occurred.

Fig. 13 shows the average value of the crack mouth opening measured for each specimen as a function of load cycles. It took 32,328 cycles for the crack to propagate from the notch at the bottom of the unreinforced specimen to the top surface and cause complete failure and separation. As for the reinforced specimen, even after 100,000 cycles, the crack could not penetrate the geogrid layer and was arrested at that location.

As was observed in the case of monotonic loading, it was noted that the geogrid reinforced samples cracked before the plain concrete during the early cycles of loading as shown in Fig. 14. However, after initial cracking, the plain concrete samples showed a big jump in the crack opening unlike the geogrid reinforced samples where such jumps were controlled by the presence of the reinforcement layer. For the specimen designation in Fig. 14, the first letter P stands for plain concrete (control samples) and G stands for geogrid reinforced samples. The second acronym, c stands for cyclic loading. The third number is the replicate number.

4. FE model calibration and sensitivity analyses

The experimental results were used to calibrate FE numerical models for conducting sensitivity analyses. Fig. 15 shows a comparison between the calibrated FEM numerical predictions and

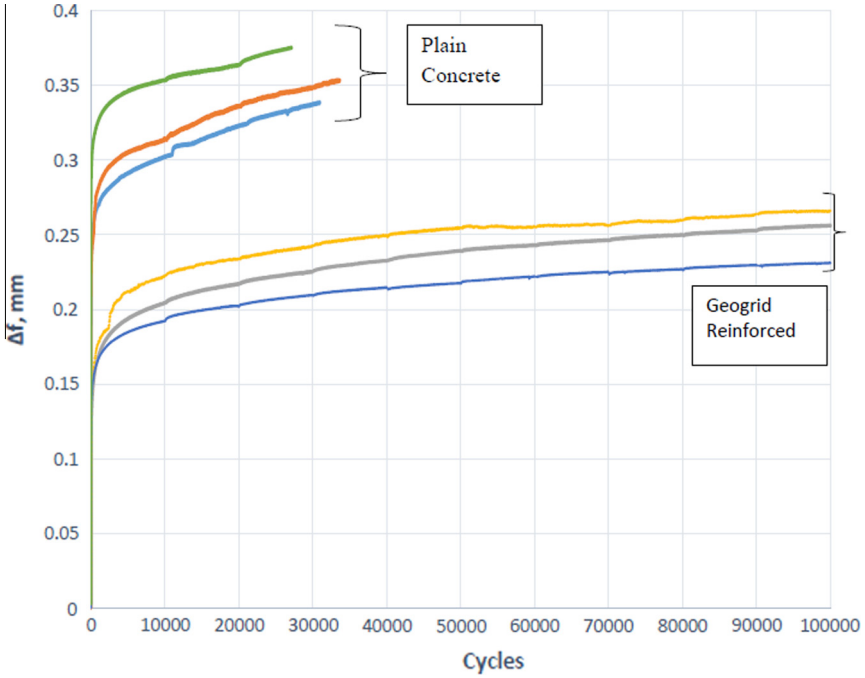

Fig. 13. Δf vs. number of cycles for each specimen.

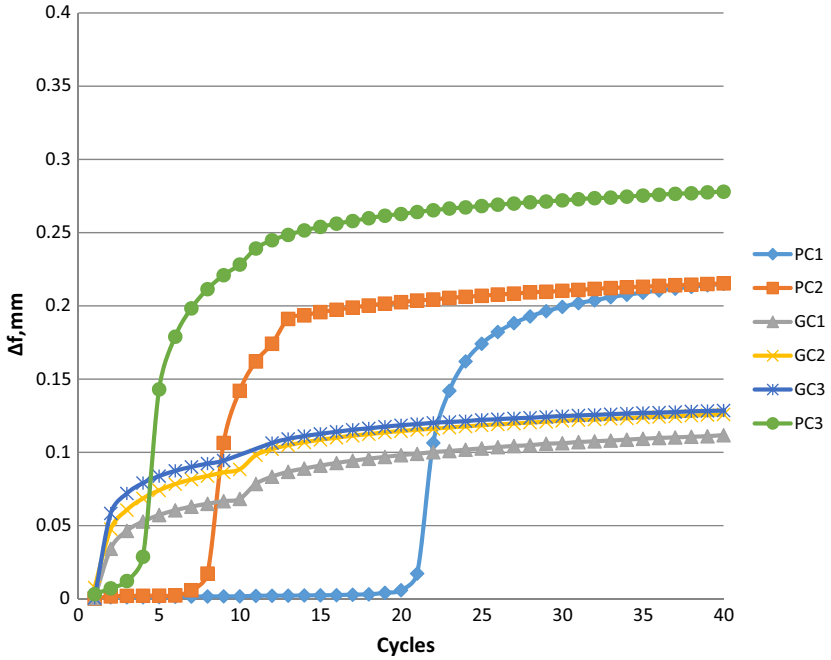

Fig. 14. Δf vs. number of cycles for the initial cracking phase.

the average experimental results for the load displacement curves corresponding to the direct tension test of a geogrid reinforced specimen. The calibrated model parameters are then employed to study the effects of temperature changes in concrete overlays.

For that purpose, two FEM models similar to the one depicted in Fig. 2a were developed: plain concrete and geogrid reinforced. The bottom of each specimen is assumed fixed, and a cyclic triangular loading having a peak displacement load of 0.0045 mm is applied on the top of the specimen. The peak displacement load is selected to simulate the effects of a 3.75 °C thermal differential. Figs. 16 and 17 show the peak stress and strain values predicted by the FEM model as a function of the number of loading cycles. It is noted that the plain concrete model witnessed a drop in the stress after initial cracking and the decrease continued until model failure (~8 cycles); this can be seen also from the strain curve which starts to increase dramatically after initial cracking. On the other hand, the peak stresses and strains in the geogrid reinforced model maintained constant values after initial cracking and until model failure (~18 cycles).

Fig. 18 shows the FE model developed to simulate the flexure test. The concrete overlay was modeled with eight nodes three dimensional elements assigned using the nonlinear, multi-axial

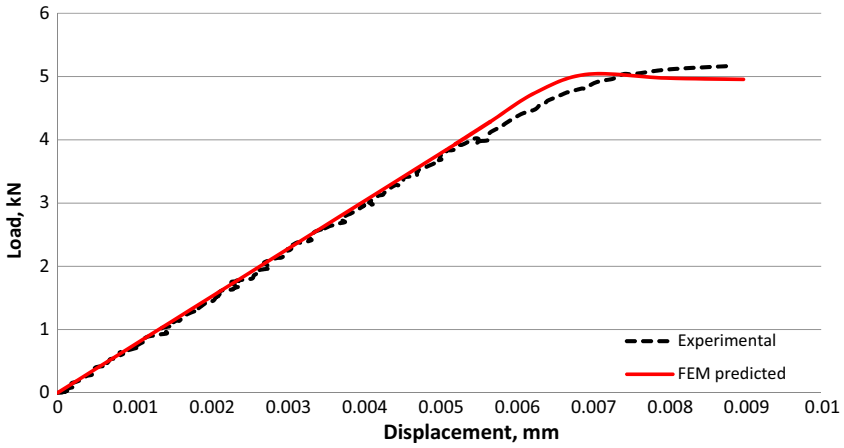

Fig. 15. FE model prediction vs. experimental results for the direct tension test of the geogrid reinforced specimen.

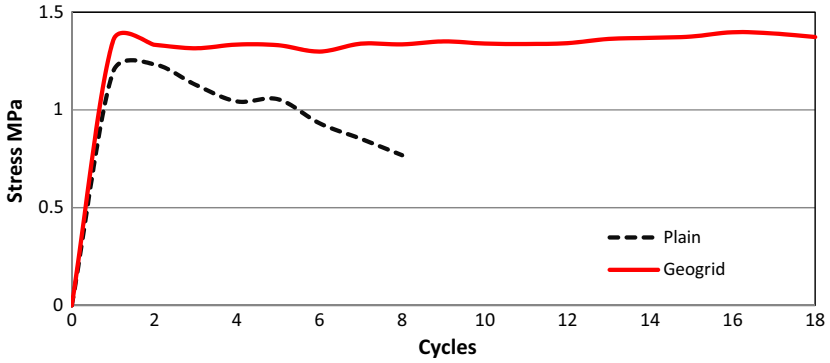

Fig. 16. Peak FEM predicted stress vs. number of cycles for plain and reinforced concrete models subject to simulated thermal loads.

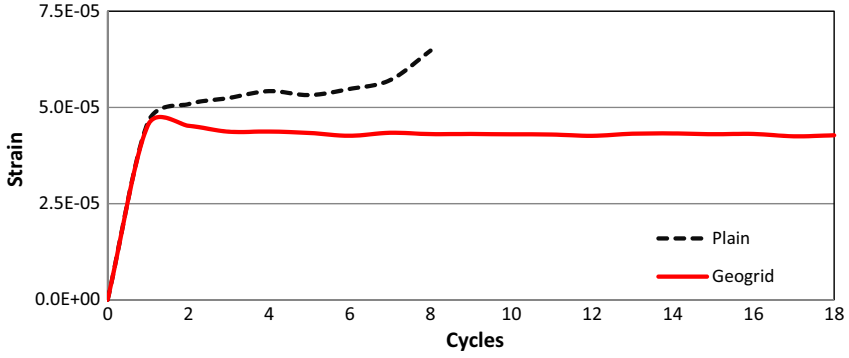

Fig. 17. Peak FEM predicted strain vs number of cycles for plain and reinforced concrete models subject to simulated thermal loads.

constitutive concrete model. The steel plate and the geogrid layer were modeled with linear elastic material. The maximum mesh size was selected to be 5 mm. Loading was applied at a rate of 0.216 kN/s, and an incremental solution process was adopted using the full Newton iteration method. Interface elements were used to define contact conditions between different layers. The contacts of upper and lower layer of concrete with geogrid were governed by the vertical and horizontal adhesion and friction coefficient between concrete and geogrid. Furthermore, interface elements were used to model the interaction between the steel loading plate and the overlay and overlay and the rubber base.

The model was first calibrated using the experimental results and then employed to investigate the effect of varying the geogrid layer location on the overall performance of the concrete overlay.

Three locations were studied: 1/3, 1/5 and 1/8 the depth. The analysis was done for analyzing the pre-cracking phase behavior only. Fig. 19 shows a comparison of the force vs Δf curves between the three studied cases. It is noted that the location of the layer did not impact the section capacity. However, it is observed that placing the geogrid layer at one third the depth of the overlay resulted in limiting the value of Δf to a minimum when compared with the other two scenarios.

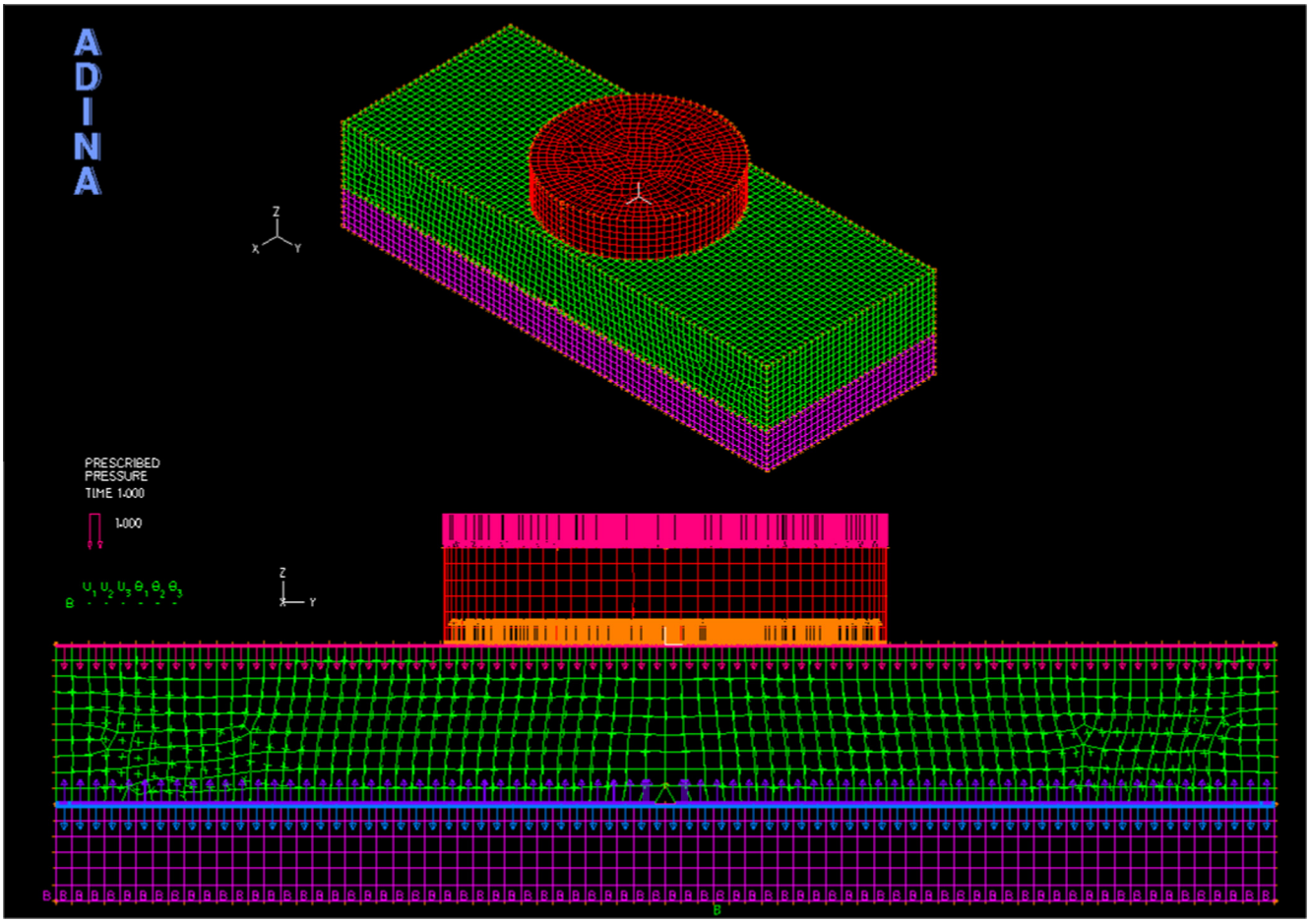

Fig. 18. FE Model simulating the flexure test.

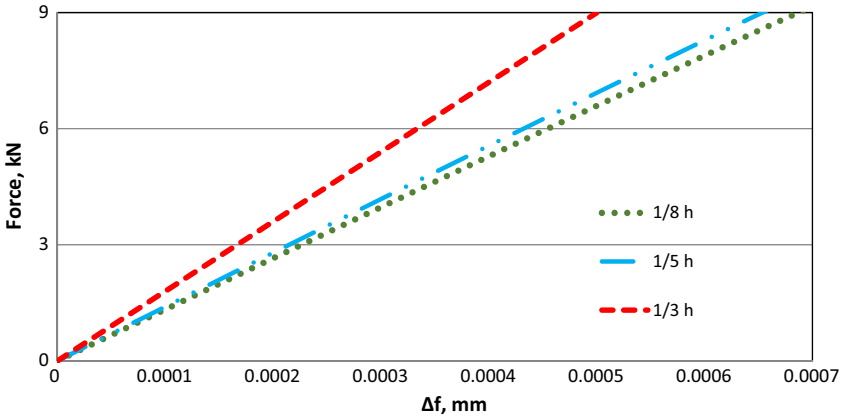

Fig. 19. FEM simulated force vs Δf curves for different geogrid locations in the specimen.

5. Conclusions

This study investigated the use of geogrids as main reinforcement in thin concrete overlays. Plain and reinforced Portland cement concrete samples with the same mix design were tested under direct tension monotonic loading and under flexure monotonic/cyclic loading. Based on the findings from all tests, the benefits of the inclusion of the geogrid in concrete overlays can be summarized as follows:

- Different failure modes were observed for specimens under direct tension. Plain samples exhibited brittle failure however the geogrid reinforcement adds a substantial post-cracking ductility where reinforced samples showed an increase in strength after cracking as well as larger deformations.
- In terms of fracture energy, the reinforced samples were more resilient to cracking than the plain concrete ones due to the interlocking phenomena that occur between the aggregates and the geogrid.

- Slabs tested under monotonic loading showed that the inclusion of geogrids results in early initial cracking and the values of Δf of the geogrid samples in the pre-cracking phase are greater than the plain concrete. However, after initial cracking the geogrid controls the rate of crack opening; whereas in plain concrete samples the Δf values are much higher than the reinforced sample.
- Two different modes of failure were observed for the slab samples under monotonic loading. The plain concrete samples completely failed and split in half whereas the crack in the geogrid samples did not reach the top face of concrete.
- Slabs tested under cyclic loading showed that the inclusion of geogrids results in substantial improvement in the performance and service life of the overlays in terms of the required number of cycles for failure and crack opening/propagation.

Acknowledgements

The authors would like to acknowledge the University Research Board (URB) at the American University of Beirut for partially funding this research.

References

[1] P.C. Taylor, S.H. Kosmatka, G.F. Voigt, Integrated Materials and Construction Practices for Concrete Pavement: A State-of-the-Practice Manual, National Concrete Pavement Technology Center/Center for Transportation Research and Education Iowa State University, Ames, 2007.
[2] I. Gonzalez-Torre, M.A. Calzada-Perez, A. Vega-Zamanillo, D. Castro-Fresno, Evaluation of reflective cracking in pavements using a new procedure that combine loads with different frequencies, Constr. Build. Mater. 75 (2015) 368–374.
[3] D.H. Chen, M. Won, CAM and SMA mixtures to delay reflective cracking on PCC pavements, Constr. Build. Mater. 96 (2015) 226–237.
[4] I.L. Al-Qadi, D.A. Morian, S.M. Stoffels, M. Elseifi, G. Chehab, T. Stark, Synthesis on Use of Geosynthetics in Pavements and Development of a Roadmap to Geosynthetically-Modified Pavements, Federal Highway Administration, 2008.
[5] A. Khodaii, S. Fallah, Effects of geosynthetic reinforcement on the propagation of reflection cracking in asphalt overlays, Int. J. Civ. Eng. 7 (2) (2009) 131–140.
[6] A.H. De Bondt, Anti-Reflective Cracking Design of (Reinforced) Asphalt Overlays, Delft University of Technology, Delft, 1998.
[7] J. Kim, W.G. Buttlar, Analysis of reflective crack control system involving reinforcing grid over based-isolating interlayer mixture, J. Transp. Eng. (ASCE) (2002) 375–384.
[8] E.M. Palmeira, F. Tatsuoka, R.B. Bathurst, P.E. Stevenson, J.G. Zornberg, Geosynthetics materials and applications for soil reinforcement and environmental protection works, Electron. J. Geotech. Eng. 13 (Special Issue State of the Art in Geotechnical) (2008) 1–38.
[9] S. Maxwell, W. Kim, T.B. Edil, C.H. Benson, Effectiveness of Geosynthetics in Stabilizing Soft Subgrades, Madison, WI, 2005.
[10] R.M. Koerner, Designing with Geosynthetics, third ed., Prentice Hall, Upper Saddle River, NJ, 1994.
[11] J. Zornberg, J. Prozzi, R. Gupta, R. Luo, J.S. McCartney, J.Z. Ferreira, C. Nogueira, Validating Mechanisms in Geosynthetic Reinforced Pavements, Austin, Texas, USA, 2008.
[12] K. Rajeshkumar, N. Mahendran, R. Gobinath, Experimental studies on viability of using geosynthetics as fibers in concrete, Int. J. Appl. Eng. Res. (2010) 15–28.
[13] J. Norambuena-Contreras, I. Gonzalez-Torre, D. Fernandez-Arnau, C. Lopez-Riveros, Mechanical damage evaluation of geosynthetics fibres used as anti-reflective cracking systems in asphalt pavements, Constr. Build. Mater. 109 (2016) 47–54.
[14] J. Norambuena-Contreras, I. Gonzalez-Torre, Influence of geosynthetic type on retarding cracking in asphalt pavements, Constr. Build. Mater. 78 (2015) 421–429.
[15] J. Kwon, E. Tutumluer, Geogrid base reinforcement with aggregate interlock and modeling of associated stiffness enhancement in mechanistic pavement analysis, J. Transp. Res. Board 2116 (2009) 85–95.
[16] S.B. Dhule, S. Valunjkar, S. Sarkate, S. Korrane, Improvement of flexible pavement with use of geogrid, Electron. J. Geotech. Eng. (2011) 269–279.
[17] Z. Guo, Q. Zhang, Prevention of Cracking Progress of Asphalt Overlayer with Glass Fabric, Liege, Belgium, 1993.
[18] X. Tang, S. Kim, G.R. Chehab, Laboratory study of geogrid reinforcement in Portland cement concrete, RILEM International Conference on Cracking in Pavements, Chicago, Illinois, USA, 2008.
[19] F. EL Meski, G. Chehab, Flexural behavior of concrete beams reinforced with different types of geogrids, J. Mater. Civil Eng. 26 (8) (2014).
[20] S. Swaddiwudhiponga, H.-R. Lu, T.-H. Wee, Direct tension test and tensile strain capacity of concrete at early age, Cem. Concr. Res. 33 (2003) 2077–2084.
[21] W. Zheng, A. Kwan, P. Lee, Direct tension test of concrete, ACI Mater. J. (2001) 63–71.
[22] M. Saito, S. Imai, Direct tensile fatigue of concrete by the use of friction grips, ACI J. (1983) 431–437.
[23] N. Xie, W. Liu, Determining tensile properties of mass concrete by direct tensile test, ACI Mater. J. (1989) 214–219.
[24] ADINA, Theory and Modeling Guide Volume I: ADINA, ADINA R&D, Inc, Watertown, MA, 2012.